Journal of Polymer Research (2022) 29:519
https://doi.org/10.1007/s10965-022-03373-z

ORIGINAL PAPER

PAAm/CMC/nanoclay nanocomposite hydrogel: understanding the influence of initiators on the chain-growth mechanisms

Renan da Silva Fernandes[1] · Fabrício Cerizza Tanaka[1] · Carlos Roberto Ferreira Junior[1] · Uilian Gabaldi Yonezawa[1] · Márcia Regina de Moura[1] · Fauze Ahmad Aouada[1]

Received: 22 February 2022 / Accepted: 15 November 2022 / Published online: 23 November 2022

Abstract

In this study, heat measurements were used to investigate the influence of three initiators on the chain-growth mechanisms of polyacrylamide/carboxymethylcellulose/nanoclay nanocomposite hydrogels. All the matrices had highly interconnected porous surfaces with intercalated configurations. Swelling degree measurements were conducted to investigate the effect of the various formed chains on the physicochemical properties of these matrices. According to the findings, hydrogels synthesized using a potassium persulfate initiator had the highest water absorbency (around 40.8 ± 0.8 g.g^$^{-1}$), followed by those synthesized using sodium persulfate (38.1 ± 1.0 g.g^$^{-1}$) and ammonium persulfate initiators (34.8 ± 0.7 g.g^$^{-1}$). The nanoclay-containing nanocomposite had a similar water absorption tendency. Additionally, all the nanocomposites had a lower swelling degree than pure hydrogel because nanoclay acted as a physical crosslinker in the polymeric matrix, decreasing the chain elasticity and water sorption ability. Different physicochemical properties were then generated due to the difference in polymerization mechanisms. Chain combination was the preferred termination mechanism for the polymerization of the hydrogel with the highest water absorbency. It was also plausible to assume that chain transfer reactions favored the termination mechanisms of the polymerization of the nanocomposites synthesized using NaPS and APS initiators, generating polymeric chains with low molecular weight and reducing the water absorption capacity. The insertion of nanoclay inhibited the start of the polymerization initiation step by preventing the initiator from attacking the monomer. Thus, a better understanding of the interaction between the initiators and hydrogel components can aid in the synthesis of hybrid nanocomposites with desirable characteristics and properties.

Keywords Initiators · Closite-Na$^+$ nanoclay · Carboxymethylcellulose · Chain-growth mechanisms · Heat investigation

Introduction

Hydrogels have attracted significant attention for the development of several matrices for different applications, such as agricultural [1–3], medical [4, 5], and engineering [6, 7] fields, because of their unique properties, including biodegradability, biocompatibility, high hydrophilicity, and low-cost production. Vinyl-based monomers are the most common monomers used in hydrogel preparation [8, 9]. Since this polymerization reaction is generally initiated by heat or ultraviolet radiation [10], controlling it remains a difficult task.

Several composite or nanocomposite hydrogel formulations have been studied using a combination of natural or synthetic polymers and zeolite or nanoclay structures [11, 12]. The main goal of this interesting strategy is to maximize the synergic properties of the individual components in the final matrix, which may improve some unfavorable characteristics and consequently increase the possibility of their applications.

Chitosan, starch, alginate, lignin, carrageenan, pectin, and cellulose derivatives are some of the polysaccharides used in hydrogel synthesis [13–15] because of their interesting properties, such as biocompatibility, biodegradability, antimicrobial property, nontoxicity, and other functional properties [7]. Carboxymethylcellulose (CMC) is one of the most investigated cellulose derivatives because it possesses unique hydrophilic

✉ Fauze Ahmad Aouada
fauze.aouada@unesp.br

[1] Grupo de Compósitos e Nanocompósitos Híbridos (GCNH), Programa de Pós-Graduação em Ciência dos Materiais, São Paulo State University (Unesp), School of Engineering, Ilha Solteira, Ilha Solteira, SP 15385-000, Brazil

Scheme 1 Decomposition of the $R_2S_2O_8$ initiators and the formation of a radical specimen to start the initiation step: R = Na, K, or NH_4

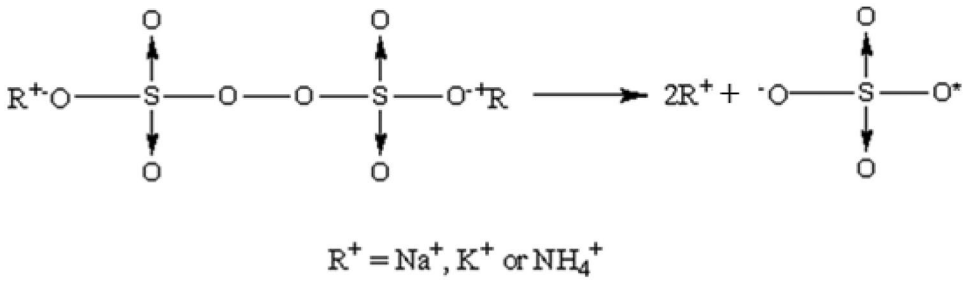

properties due to the carboxylate groups present in its backbone [16], as well as interesting characteristics such as sensitivity to external stimuli. This environmental response is very desirable for diverse applications, such as controlled release systems for agricultural, medical, or food applications.

Polyacrylamide (PAAm) is one of the most appropriate support matrices used in nanoclay-based hydrogel nanocomposites [17]. In addition to their facile, low-cost, and reproducible synthesis parameters and their wide applicability in various fields, such as drug delivery [18], agricultural inputs [19, 20], and water treatments [21], one of the main reasons for their use is that the amino groups along their chain can form hydrogen bonds with the nanoclay functional groups [22]. These interactions aid in the stabilization of nanostructures because of their anchoring.

Incorporating inorganic materials, such as nanoclays, particularly cloisite-Na^+ (Clt-Na^+), into polyacrylamide and polyacrylate networks helps improve the final properties of these matrices, such as swell capacity, mechanical resistance, and thermal stability [23, 24]. Clt-Na^+ minerals have a sheet-like structure composed of tetrahedrally arranged silicate and octahedrally arranged aluminate groups, which form platelets that are bound together by van der Waals forces [25]. Na^+ cations, which counteract the negative charges on the surface of their layers, are found in their galleries [26]. It has been widely studied because of its excellent properties, such as water adsorption capacity, cation exchange, and high specific surface area [27].

The objective of this study was to investigate the influence of the sodium persulfate (NaPS), potassium persulfate (KPS), and ammonium persulfate (APS) initiators on the chain-growth mechanism of hydrogels made from polyacrylamide (PAAm), CMC, and nanoclay Clt-Na^+ and how it affected the swelling degree (SD) of these nanocomposites. The hydrogel structure was characterized using Fourier-transform infrared spectroscopy (FTIR), X-ray diffraction (XRD), and scanning electronic microscopy (SEM) techniques. Although the influence of several initiators on the formation and the properties of hydrogels has already been reported [28–31], to the best of our knowledge, there is a lacune of understanding of how the type of initiator affects the chain-growth mechanism. For instance, Zhang et al. [28] investigated the redox-polymerization mechanisms of polyacrylamide hydrogels. They concluded that the use polyetheramine initiator could promote a more homogeneous distribution of crosslinking points and energy dissipation, improving mechanical properties. Bel'nikevich et al. [29] studied the gelation kinetics of novel poly(acrylic acid) hydrogels crosslinked using two different ammonium persulfate initiator systems. The effect of the initiator systems used in the acrylamide and their derivatives on the gel inhomogeneity was firstly reported by Orakdogen and Okay [30]. In this way, the main objectives of these references focus on the characterization of properties of these different matrices and not on the chain-growth mechanisms.

Therefore, this study aims to determine how the initiator system efficiency affects the relationship between the molecular weight of the chains and the water absorption capacity of these nanocomposites. As shown in Scheme 1, the breaking of the O–O chemical bonds in the NaPS, KPS, or APS radicals generates two $SO^{4-\bullet}$ free radicals per molecule. Therefore, the time and efficiency of the initiation step caused by the interaction between the $SO^{4-\bullet}$ radical and the vinyl monomers can affect both the polymeric chain size and the number of hydrophilic groups, as well as the water absorption properties of these nanocomposites.

Experimental

Materials

Acrylamide (AAm), N,N,N',N'-tetramethylenediamine (TEMED), and KPS ($K_2S_2O_8$) and APS ($(NH_4)_2S_2O_8$) initiators were purchased from Sigma-Aldrich. CMC (Mv = 114.000 g.mol^−1) and the NaPS ($Na_2S_2O_8$) initiator were obtained from Synth-Brazil. N,N'-methylenebisacrylamide (MBAAm) was acquired from Vetec-Brazil, and nanoclay Clt-Na^+ was obtained from Southern Clay Products®. All reagents were used as received.

PAAm/CMC/Clt-Na^+ nanocomposite hydrogel synthesis

PAAm/CMC/Clt-Na^+ nanocomposite hydrogels were synthesized via free radical polymerization (Scheme 2), as recently described by our group [23, 24]. Initially, 0.3 g of CMC (or 1.0 mass/%) was solubilized into 27 mL of distilled water under magnetic stirring. Thereafter, Clt-Na^+ (10

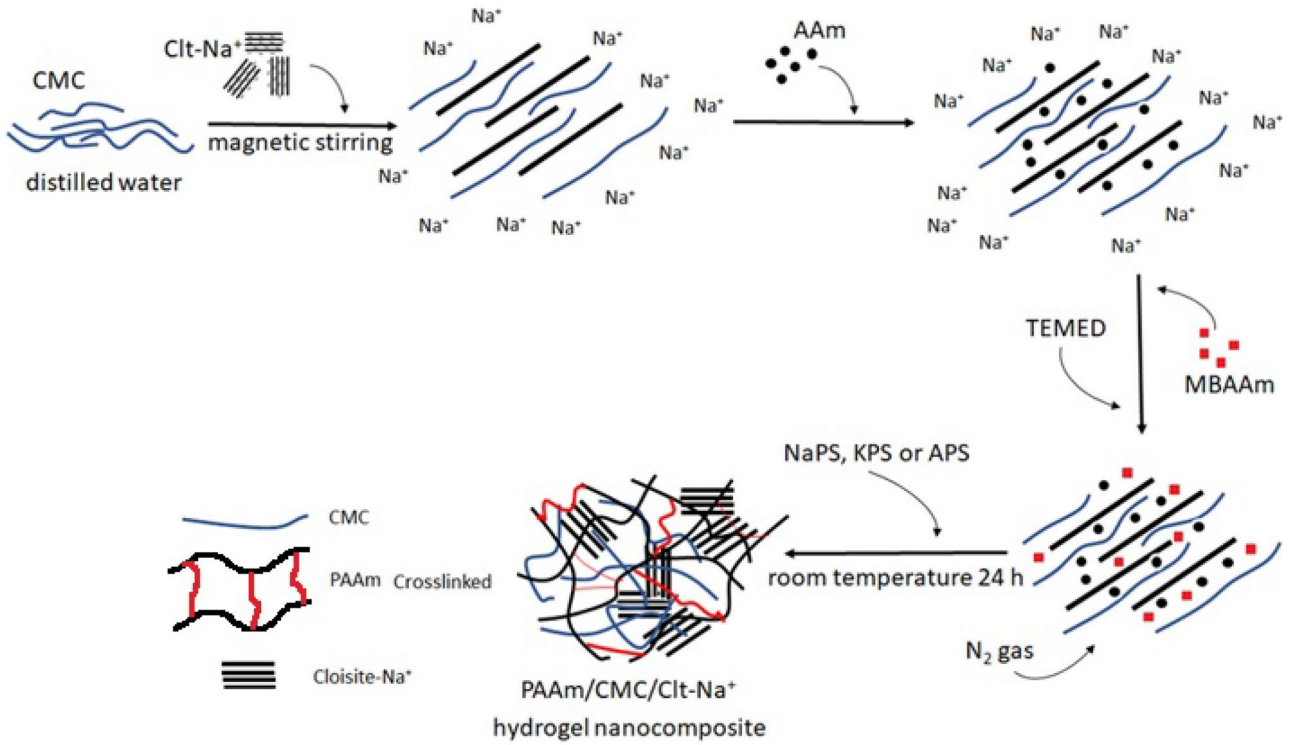

Scheme 2 Schematic representation of the formation of the PAAm/CMC/Clt-Na^+ nanocomposite hydrogels using different initiators

mass/% in relation to AAm + CMC mass) was dispersed into the CMC solution with magnetic stirring for 60 min. Sequentially, 1.8 g of AAm (or 6.0 mass/%), 0.078 g of MBAAm (C_{final} = 16.9 mmol L^−1), and 1.0 mL of the 0.2 mol L^{-1} TEMED solution (C_{final} = 6.67 mmol L^−1) were added to form a homogeneous solution. The system was then closed and maintained under a nitrogen atmosphere for 20 min to remove the oxygen dissolved in the solution. Finally, KPS, NaPS, or APS (C_{final} = 3.5 mmol L^−1) was added to start the polymerization reaction. The final solution was inserted into a mold (made up of two acrylic plaques separated by a 2 mm thick rubber spacer) and kept at room temperature for 24 h. Finally, the nanocomposites were removed and purified by dialysis for 7 days to remove all unreacted reagents.

Fourier transform infrared spectroscopy analysis

FTIR spectra were obtained on a Nicolet-NEXUS 670 FTIR spectrophotometer, operating in the spectral range of 4000–400 cm^−1. The samples were dried, pulverized, and mixed with KBr to form pellets.

X-ray diffraction analysis

XRD profiles of the powder samples were obtained using a diffractometer (Shimadzu-XRD-6000) equipped with CuK_α radiation (λ = 0.154 nm) in a scan range of 2θ = 5°–50° at 1°/min, 40 kV, and 30 mA. The interlayer spacing values (d_{001}) were calculated using Bragg's law $n.\lambda = 2.d.\sin\theta$ [32].

Scanning electron microscopy

SEM micrographs of the samples were obtained using a ZEISS EVO LS15 electronic microscope operating at 20 kV. The hydrogels were frozen in liquid nitrogen and freeze-dried at − 55 °C until constant weight using a lyophilizer (model Enterprise II Terroni) after being allowed to swell in distilled water until the equilibrium stage. Finally, the samples were coated with a thin gold layer before observation by SEM.

Swelling degree

The SD values of the matrices were measured at room temperature using gravimetric analysis. After dialysis, the samples were cut into 26 mm diameter circles and dried in an oven at 40 ± 1 °C for 24 h. The samples were subsequently immersed into 20 mL of distilled water and weighed until constant mass. The SD values were calculated using Eq. 1 [33]:

$$SD = \frac{M_t}{M_d} \quad (1)$$

where M_t and M_d are the mass of the swollen and dried hydrogels, respectively.

The equilibrium stage of the samples was achieved when the SD values remained constant. All samples reached equilibrium after 48 h. The equilibrium point in the swelling phenomenon occurs due to the balance between the elastic force within the network structure of the hydrogel and the osmotic pressure outside [34].

Kinetic parameters

The kinetic parameters of the hydrogels and their nanocomposites were calculated from the slope and intercept of ln(Mt/Meq) *versus* ln(t) plots obtained based on the Ritger and Peppas [35] model using Eq. 2:

$$\frac{M_t}{M_{eq}} = kt^n \tag{2}$$

where M_{eq} is the mass of the hydrogel at equilibrium state, k is the swelling constant, and n is the swelling exponent.

When the n values are between 0.5 and 1, the water uptake mechanism is governed by anomalous transport (or non-*Fickian* diffusion); when the n values are close to 0.5 and 1, the mechanisms are governed by *Fickian* diffusion and Case II transport, respectively [36].

Results and discussion

Fourier transform infrared spectroscopy

Table 1 shows the main spectroscopic assignments obtained for the AAm [24, 37–39], CMC [24, 37–40], and Clt-Na^+ specimens [24, 41–43]. Regardless of the initiator used, all the PAAm/CMC hydrogels (Fig. 1a, b) displayed a wide band between 3730 and 2880 cm^{-1} with peaks centered at 3438 and 3169 cm^{-1}, which correspond to the O–H and N–H stretching modes of CMC and AAm, respectively. Overlapping of the asymmetric stretching of the COO, CH_2, and C–O–C groups belonging to the CMC, C = O, and C = C stretchings, respectively, and the N–H bending belonging to AAm is found in the 1675–1610 cm^{-1} region. Another significant peak corresponding to the C = C bond of AAm was observed at 985 cm^{-1}. All the hydrogel spectra displayed a CMC characteristic peak centered at 1417 cm^{-1} (–COO bending and C–O–O stretching). The absence of the C = C peaks in the PAAm/CMC hydrogel spectra confirmed its formation.

Figure 1 shows three characteristic Clt-Na^+ peaks at 1045, 917, and 465 cm^{-1}, which correspond to the Si–O stretching and Al–OH–Al and Si–O–Si bending [24, 42, 43], respectively, in all the PAAm/CMC/Clt-Na^+ nanocomposites. In addition, in the nanocomposite spectra, the intensity of the peak at 1115 cm^{-1} corresponding to the–CH–O–CH_2– group [24, 37–39] present in the PAAm/CMC hydrogel decreases. The peak at 1640 cm^{-1} (attributed to the overlapping of the C = O stretching and N–H bending belonging to PAAm and the $–COO^-$ stretching and CH_2 bending belonging to CMC) [24, 37–40] found in the PAAm/CMC hydrogels was displaced to 1670 cm^{-1} in the PAAm/CMC/Clt-Na^+ nanocomposites. Based on these observations, we hypothesized a scheme (Scheme 3) that depicts the possible interactions point between the nanoclay and polymeric matrix.

Table 1 Main spectroscopic attributions of CMC, AAm, and raw Clt-Na^+

Carboxymethylcellulose		Acrylamide		Cloisite-Na^+	
Peak (cm^{-1})	Assignment	Peak (cm^{-1})	Assignment	Peak (cm^{-1})	Assignment
3438	O–H stretching	3380–3185	N–H stretching	3620	OH sctructural stretching
2917	C-H stretching	2812	C-H stretching	3456	OH interlayer stretching
1618	-COO asymmetric stretching, CH_2 bending, C–O–C stretching	1675	C = O and C = C stretchings	1640	OH water bending
1417	-COO bending, C-O–O stretching	1610	N–H bending	1045	Si–O stretching
1326	-CCH and -OCH coupled bend CH_2 rocking vibration	1431	CH_2 bending	917	Al–OH–Al bending
1057	CH–O–CH_2 stretching	1350	C-H bending	795	Si–O–Al vibration
		1277	C-N stretching	524	Si–O–Al vibration
		1139	C–C symmetric stretching	465	Si–O–Si bending
		1050	C–C asymmetric stretching		
		992	Out of plan C = C–H bending		
		960	Out of plan C = C bending		
		700–619	N–H out-of-plane bending		

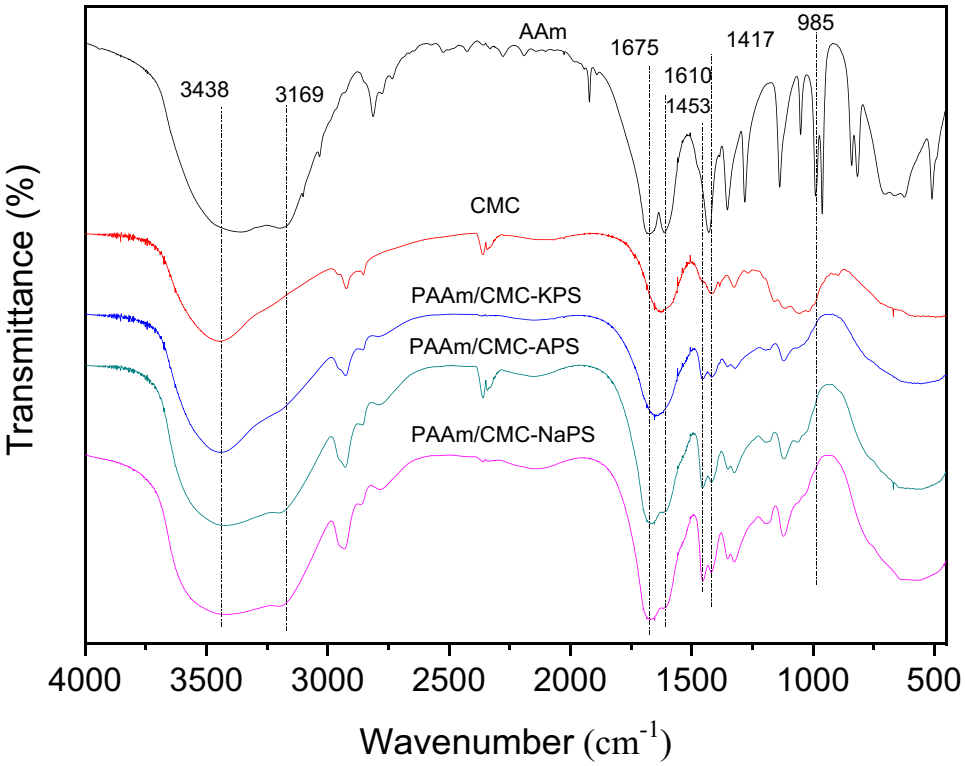

(a)

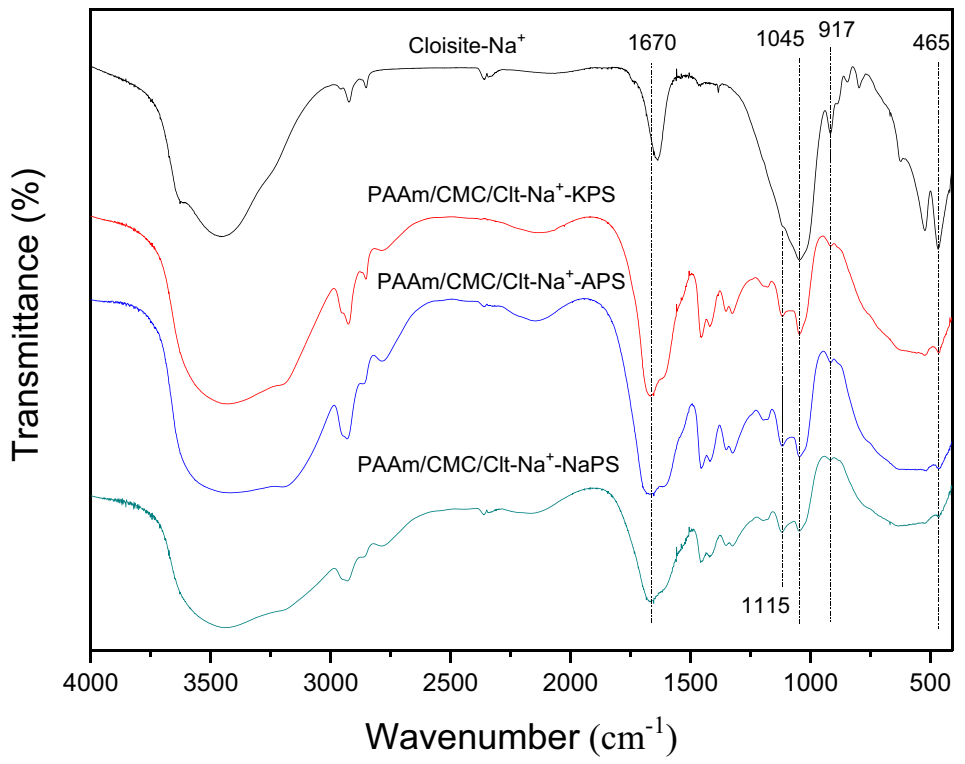

(b)

Fig. 1 FTIR spectra of **a** CMC, AAm, and PAAm/CMC, **b** Clt-Na^+ and the PAAm/CMC/Clt-Na^+ synthesized using different initiators

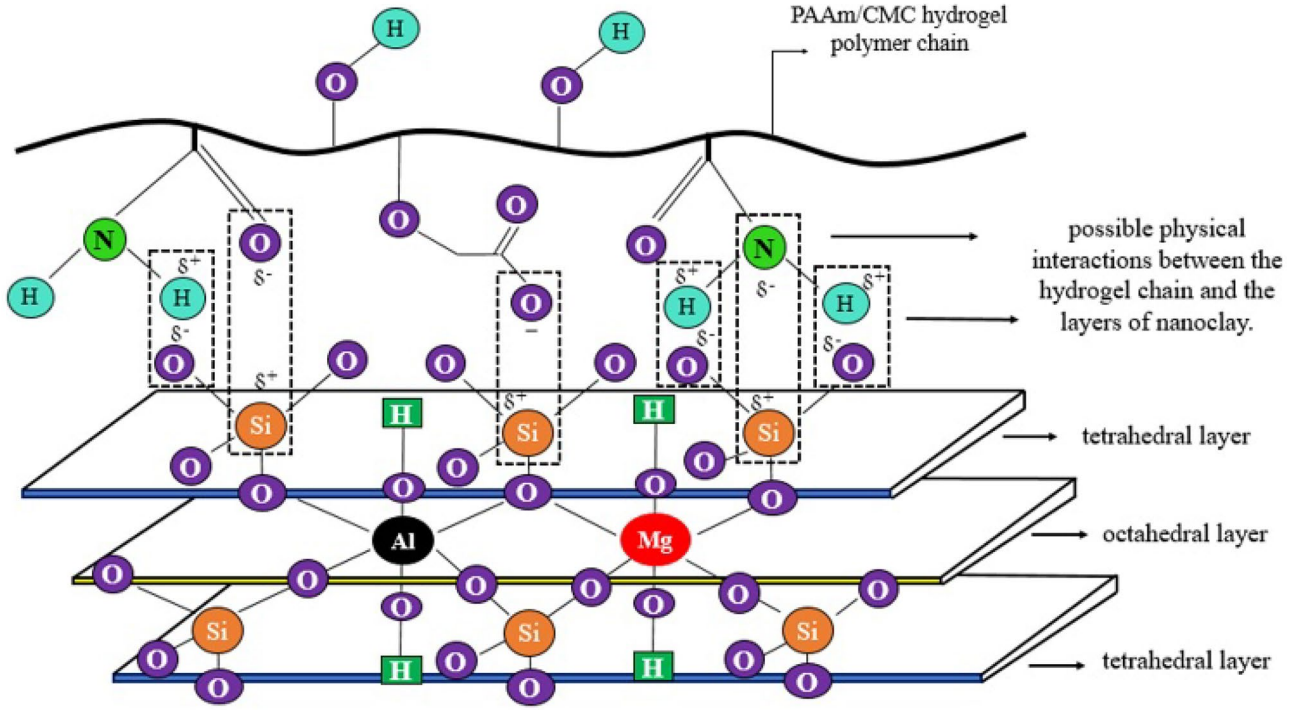

Scheme 3 Possible interaction sites between the hydrogel chain and nanoclay

X-ray diffraction

Figure 2 shows an intense diffraction peak at $2\theta = 7.40°$ in the XRD pattern of the raw Clt-Na^+, which corresponds to a basal spacing (d_{001}) of 1.19 nm. This value is very similar to the value reported by Mirzataheri et al. [44] and Brantseva et al. [45].

The displacement of this diffraction peak from $2\theta = 7.40°$ to 6.25° (or $d_{001} = 1.41$ nm) in the XRD patterns of the hydrogel nanocomposites is caused by the opening of the nanoclay layers, suggesting its intercalation into hydrogel chains, as we hypothesized in Scheme 4. A minor shift in the same diffraction peak was previously oberved by our research group [43] for intercalated nanocomposites based on poly(methacrylic acid) hydrogel and nanoclay cloisite-Na^+. The maximization in the intercalation process observed here is probably related to the presence of the CMC polysaccharide.

The amorphous characteristic of the PAAm/CMC hydrogel is preserved in all the nanocomposites even after nanoclay addition. Due to the similarity in the XRD patterns, it was not possible to affirm that the type of initiator modifies their crystallinity. The amorphous regions inside hydrogel nanocomposites increased the sorption capacity of these matrices. Thus, preserving this property is vital, as these nanocomposites could be used as an adsorbent material to remove pesticides from contaminated water [46].

Scanning electron microscopy

Figure 3 shows the micrographs of the PAAm/CMC and PAAm/CMC/Clt-Na^+ nanocomposites prepared using three different initiators. The presence of hydrophilic groups and the pore size are both known to influence the expansion of hydrogel chains [47]. All PAAm/CMC hydrogels initiated with NaPS (Fig. 3a), KPS (Fig. 3c), and APS (Fig. 3e) had highly interconnected porous surfaces. Similar morphologies were reported, for instance, by Meng et al. [48] for highly flexible interconnected Li^+ ion-sieve porous hydrogels and by Cao et al. [49] for eco-friendly porous double-network hydrogel derived from keratin. Although the highest amount of pores had good interconnection, the presence of some closed pores is expected because of the lyophilization process. In this process, when the molecules of water are sublimed, a force (thermodynamic process) presses the pore walls, thickening them. These morphological properties are extremely important because they help the matrix absorb water, which is facilitated by interactions with the hydrophilic groups of the hydrogel [50].

It was discovered that regardless of the initiator used, the pores retracted when nanoclay was added to the hydrogels (Fig. 3b, d and f), compared to the matrix without nanoclay. This effect is due to the nanoclay acting as a physical crosslinker of the polymeric chains [24], which justifies the SD reduction, as will be further discussed.

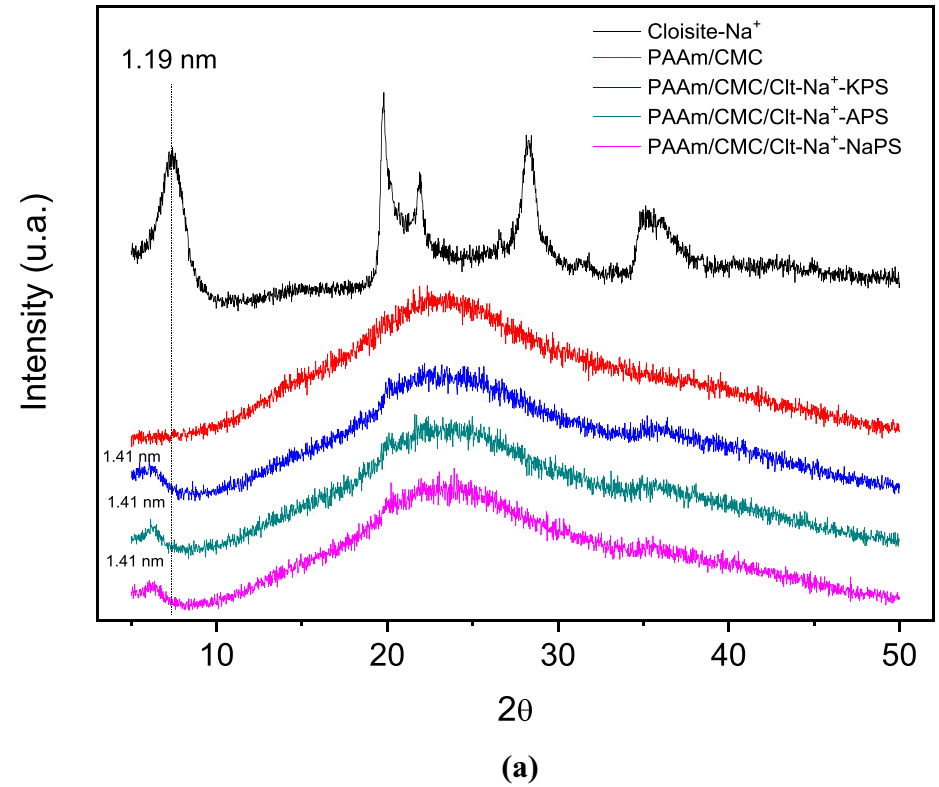

(a)

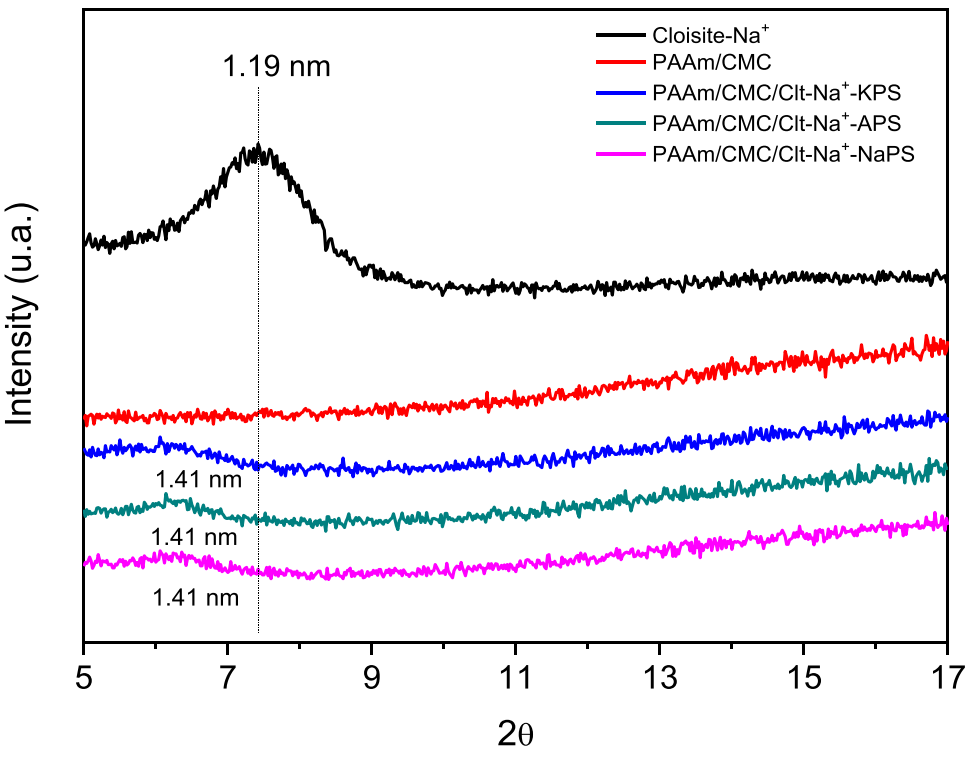

(b)

Fig. 2 **a** XRD patterns of the nanoclay and nanocomposite hydrogels prepared using different initiators, **b** range of 2 θ = 5-17º, indicating the intercalation region

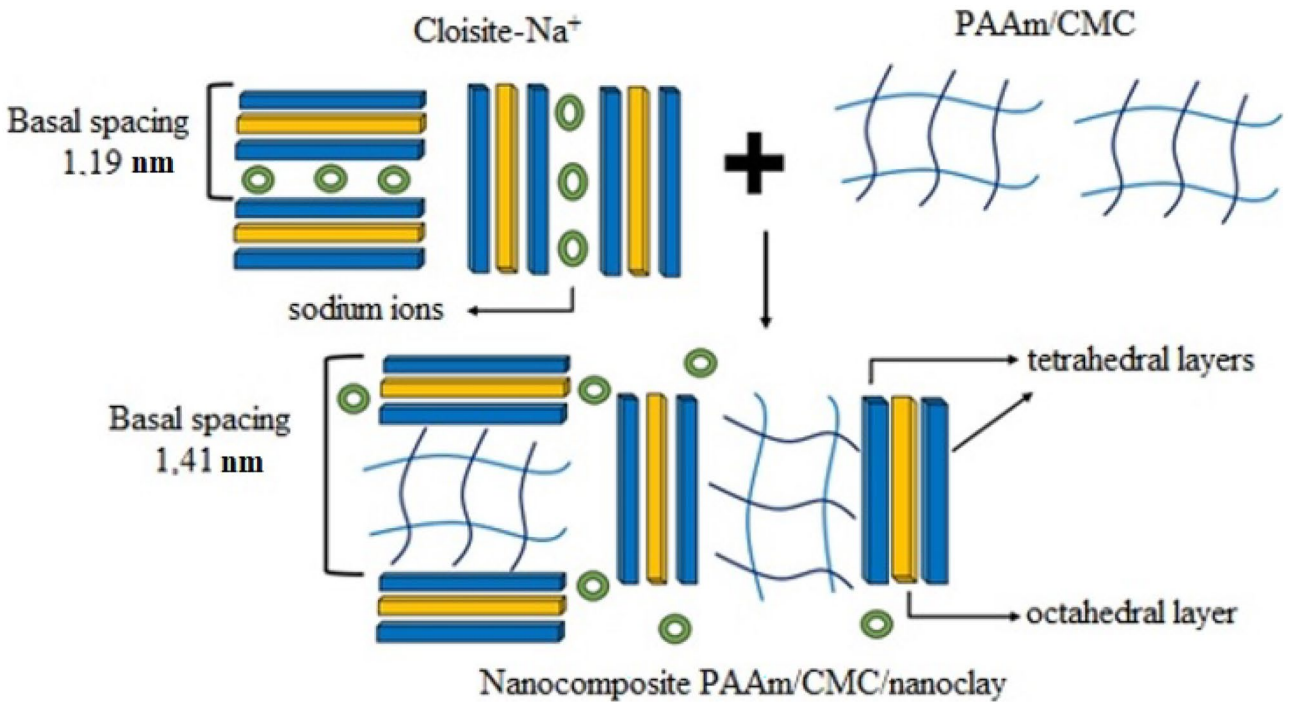

Scheme 4 A hypothetic model of hydrogel conformation into a nanoclay structure

Swelling degree

The swelling degree was investigated to further understand the synthesis mechanism of these nanoclay-containing matrices, which were synthesized with three different initiators.

Figures 4 and 5 shows that the hydrogels synthesized with the KPS initiator had the highest swelling capacity, followed by those synthesized with the NaPS and APS initiators, indicating that the KPS initiator maximized the growth of the polymer chains and increasing the number of available hydrophilic groups that can interact with water molecules. This makes the formation of polymeric chains more thermodynamically favorable, allowing them to grow faster and absorb more water, resulting in chains with higher molecular weights (or with higher lengths) and more hydrophilicity. Based on these results, the nanocomposites synthesized by the KPS initiator probably had a slower velocity in the initiation step.

According to Umar et al. [51], the synergic effect of the rapid decomposition of the initiator and the high temperature of the polymer solution may favor the termination step via chain transfer mechanism. In this case, the matrix will be made up of polymeric chains with low molecular weight and a small number of hydrophilic groups, which will decrease their expansion capacity [52], as confirmed by their decreased SD values (Fig. 5). A slower initiation stage can reduce the termination stage. In this condition, the termination mechanism is most likely to occur through chain combination [53]. We hypothesized that the synthesis with the KPS initiator had the slowest termination stage, indicating that this synthesis requires more time to lose heat than the syntheses with the other initiators.

The decrease in swelling degree observed for all nanocomposites is probably associated with the obstruction caused by the presence of nanoclay among the initiator and monomer in the nanocomposite-forming polymeric solution, which causes a possible decrease in the chain molecular weight of the nanocomposite. These factors, which are associated with the physical crosslinking caused by nanoclay, are responsible for decreasing the chain elasticity and density of the hydrophilic groups, consequently decreasing the capacity of these nanocomposites to absorb and retain water molecules in their three-dimensional structure.

It is well-know in the literature that cross-linking density is one of the most important parameters affecting the mechanical properties of the hydrogels. For instance, Xiang et al. [54] observed that presence of inorganic clay (Laponite XLS) increased the tensile strength, elongation at break, and compressive strength of biocompatible clay/P(MEO_2MA-co-OEGMA) nanocomposite hydrogels. The amount of water absorption also has an important effect on the mechanical properties of the hydrogels. Aouada et al. [55] confirmed that modulus of elasticity and swelling degree properties of the poly(acrylamide) and methylcellulose hydrogels are inversely proportional.

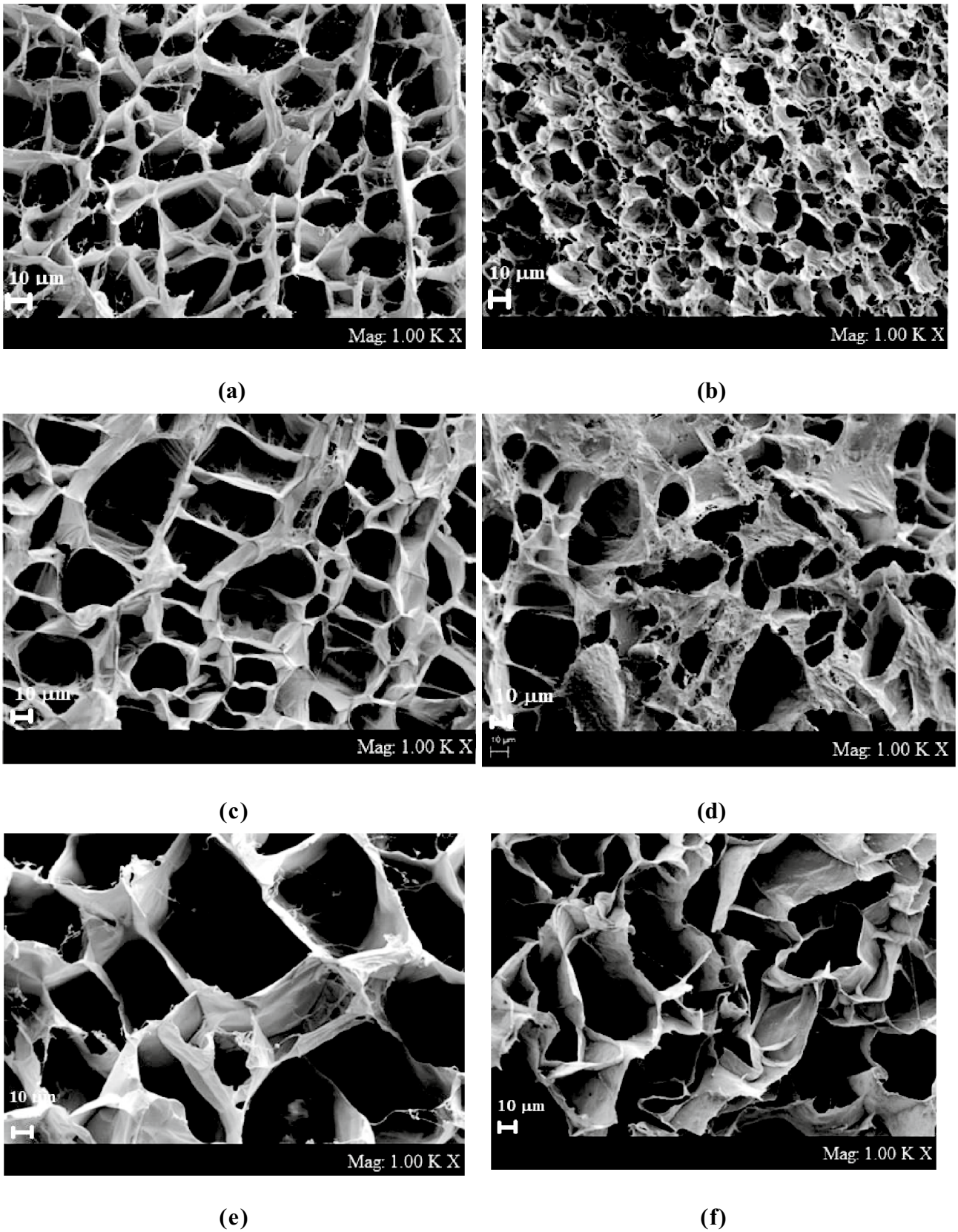

Fig. 3 SEM micrographs of **a** PAAm/CMC-NaPS, **b** PAAm/CMC/10%-Clt-Na^+-NaPS, **c** PAAm/CMC-KPS, **d** PAAm/CMC/10%-Clt-Na^+-KPS, **e** PAAm/CMC-APS, and **f** PAAm/CMC/10%-Clt-Na^+-APS. Hydrogel micrographs were obtained at 1.000 × magnification. The bar size is 10 µm, and an accelerating voltage of 7.0 kV was applied

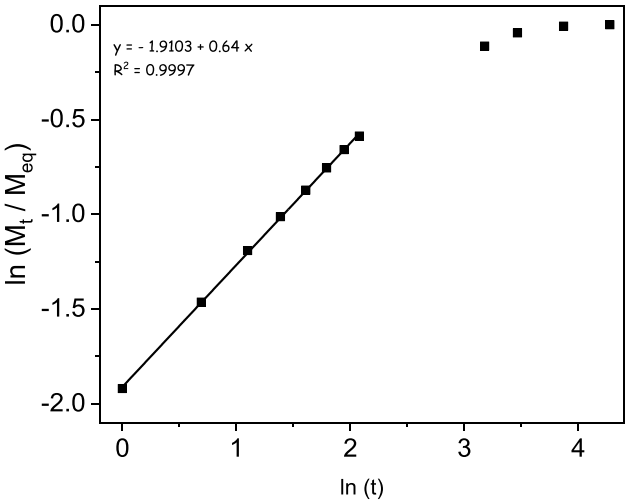

Fig. 4 Example of a swelling kinetic plots ln (M_t/M_{eq}) *vs* ln t of PAAm-CMC-NaPs hydrogel used to determine the *n* e *k* parameters

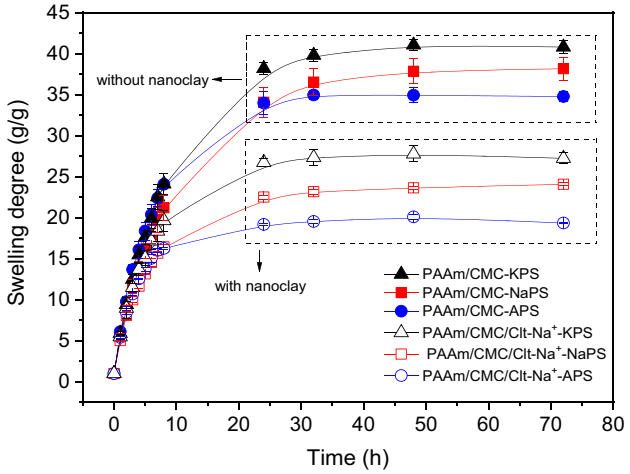

Fig. 5 Dependence of the SD of the hydrogels prepared separately using KPS, APS, and NaPS initiators as a function of time

Kinetic parameters

An example of swelling kinetic plot ln (M_t/M_{eq}) *vs* ln t, used to determine the diffusional exponent *n* and constant *k,* is shown in Fig. 4, and their values are shown in Table 2.

Equations 3 [56] and 4 [35] represent the Fick´s first and second laws. Fick´s first law indicates that the mass flux (J) of the solute depends to their rate of change concentration in relation to position, ∂C/∂x [56]. Already, the Fick´s second law is found from Fick´s first law and mass conservation.

$$J = -D\frac{\partial C}{\partial x} \tag{3}$$

where D is the diffusion coefficient.

$$\frac{\partial C}{\partial t} = D\frac{\partial^2 C}{\partial x^2} \tag{4}$$

where t is the time.

The water molecules were transported anomalously through the three compositions without nanoclay. However, when nanoclay was introduced into the polymeric matrix, the *n* values decreased, indicating *Fickian* diffusion. The same behavior was observed for hydrogels synthesized from APS initiator. This trend is related to the reduction in the elasticity of the polymeric chains [57]. The SD measurements indicated that the introduction of nanoclay increased the rigidity of the polymeric matrix. Indeed, all the nanoclay-containing nanocomposites presented a 45% reduction in water absorption.

Additionally, the incorporation of nanoclay galleries into the nanocomposites improved the velocity of water uptake by about 50%, as quantified by constant *k*. This improvement is crucial for applications that require rapid water uptake, such as the remediation of water contaminated by pollutants. Finally, from Table 2, it was possible to observe an inverse correlation between SD_{eq} and *k* parameter. For instance, polymeric matrices synthesized from the APS initiator had the highest *k* (highest water uptake velocity) parameter and the lowest SD_{eq} values (lowest water absorption).

Conclusions

In this study, PAAm/CMC/Clt-Na^+ nanocomposites were successfully synthesized, and the chain-growth mechanisms for different systems started by three initiators were investigated. The most probable interaction points between the polymeric matrix and nanoclay were identified using spectroscopic techniques. Scanning electron micrographs confirmed that all the

Table 2 Obtained SD_{eq}, *k* and *n* values of the hydrogel and nanocomposite hydrogels synthesized using different initiators

[%Clt-Na +]	KPS				NaPS				APS			
	SD_{eq} (g/g)	*n*	*k* (h^{-1})	R^2	SD_{eq} (g/g)	*n*	*k* (h^{-1})	R^2	SD_{eq} (g/g)	*n*	*k* (h^{-1})	R^2
0	40.8 ± 0.8	0.68 ± 0.01	0.14*	0.99	38.1 ± 1.0	0.64 ± 0.01	0.15*	0.99	34.8 ± 0.7	0.66 ± 0.01	0.18 ± 0.01	0.99
10	27.2 ± 0.6	0.61 ± 0.01	0.21 ± 0.01	0.99	24.1 ± 0.2	0.57 ± 0.01	0.22*	0.99	19.3 ± 0.1	0.54 ± 0.01	0.28 ± 0.01	0.98

*Standard deviation < 0.01

nanocomposites had highly interconnected porous surfaces regardless of the presence of nanoclay or the initiator type and that the pores suffered retraction because of the presence of nanoclay. Both the retraction and physical crosslinking effects of the nanoclay were confirmed by SD measurements. The XRD analysis revealed that the nanoclay was intercalated into the polymeric matrix and that the amorphous characteristics of the matrix were preserved even after nanoclay addition. Free radical polymerization reactions initiated by NaPS, KPS, or APS modified the molecular weight and hydrophilicity of the nanoclay–hydrogel nanocomposite chains. It was possible to understand how the chain-growth mechanism influenced the physicochemical properties of these matrices.

This study is very promising because controlling the chain-growth mechanisms may optimize the hydrophilic properties of these nanocomposites, increasing their applicability.

Acknowledgements The authors would like to thank UNESP, grants 2018/18697-1; 2013/03643-0; 2013/07296-2 São Paulo Research Foundation (FAPESP), and CNPq (MRM 312530/2018-8; FAA 405680/2016-3; 312414/2018-8; 316174/2021-1). This paper was possible thanks to the scholarship granted from the Brazilian Federal Agency for Support and Evaluation of Graduate Education (CAPES), in the scope of the Program CAPES-PrInt, process number 88887.310463/2018-00, International Cooperation Project number 88887.310309/2018-00. This study was financed in part by CAPES–"Finance Code 001."

Author´s contributions R.S.F, F.C.T, C.R.F.J, U.G.Y conceived, collected, and analysed the data. M.R.M supervised, and F.A.A conceptualized and supervised the manuscript. All authors wrote and contributed to manuscript revision, read, and approved the submitted version.

Data availability Not applicable.

Declarations

Conflict of interest The authors declare NO conflicts of interest or competing interests.

References

1. ALSamman MT, Sánchez J (2021) Recent advances on biobased hydrogels based on chitosan and alginate for the adsorption of dyes and metal ions from water. Arab J Chem 14:103455
2. Głowińska A, Trochimczuk AW, Jakubiak-Marcinkowska A (2019) Novel acrylate/organophosphorus-based hydrogels for agricultural applications. New outlook and innovative concept for the use of 2-(methacryloyloxy)ethyl phosphate as a multi-purpose monomer. Eur Polym J 110:202
3. Singh N, Agarwal S, Jain A, Khan S (2021) 3-Dimensional cross linked hydrophilic polymeric network "hydrogels": An agriculture boom. Agr Water Manag 253:106939
4. Eshkol-Yogev I, Gilboa E, Giladi S, Zilberman M (2021) Formulation - Properties effects of novel dual composite hydrogels for use as medical sealants. Eur Polym J 152:110470
5. Song F, Zhang J, Lu J, Cheng Y, Tao Y, Shao C, Wang H (2021) A mussel-inspired flexible chitosan-based bio-hydrogel as a tailored medical adhesive. Int J Biol Macromol 189:183
6. Sun A, He X, Ji X, Hu D, Pan M, Zhang M, Qian Z (2021) Current research progress of photopolymerized hydrogels in tissue engineering. Chinese Chem Lett 32:2117
7. Pita-López ML, Fletes-Vargas G, Espinosa-Andrews H, Rodríguez-Rodríguez R (2021) Physically cross-linked chitosan-based hydrogels for tissue engineering applications: A state-of-the-art review. Eur Polym J 145:110176
8. Tanaka FC, Junior CRF, Fernandes RS, Moura MR, Aouada FA (2021) Correlating pH and swelling degree parameters to understand the sorption and desorption process of diquat herbicide from nanocomposites based on polysaccharide and clinoptilolite. J Polym Environ 29:3389
9. Pfeifer M, Andrade FAC, Bortoletto-Santos R, Aouada FA, Ribeiro C (2021) Effect of different surface-charged lamellar materials on swelling properties of nanocomposite hydrogels. J Polym Environ 29:3311
10. Chen Y, Wang D, Mensaha A, Wang Q, Cai Y, Wei Q (2022) Ultrafast gelation of multifunctional hydrogel/composite based on self-catalytic Fe^{3+}/tannic acid-cellulose nanofibers. J Colloid Interf Sci 606:1457
11. Cimen Z, Babadag S, Odabas S, Altuntas S, Demirel G, Demirel GB (2021) Injectable and self-healable pH-responsive gelatin–PEG/laponite hybrid hydrogels as long-acting implants for local cancer treatment. ACS Appl Polym Mat 3:3504
12. Biswas S, Fatema J, Debnath T, Rashid TU (2021) Chitosan–clay composites for wastewater treatment: A state-of-the-art review. ACS ES&T Water 1:105
13. Abudula T, Colombani T, Alade T, Bencherif SA, Memić A (2021) Injectable lignin-co-gelatin cryogels with antioxidant and antibacterial properties for biomedical applications. Biomacromol 22:4110
14. Yan X, Rahman S, Rostami M, Tabasi ZA, Khan F, Alodhayb A, Zhang Y (2021) Carbon quantum dot-incorporated chitosan hydrogel for selective sensing of Hg^{2+} ions: Synthesis, characterization, and density functional theory calculation. ACS Omega 6:23504
15. Pandit AH, Nisar S, Imtiyaz K, Nadeem M, Mazumdar N, Rizvi MMA, Ahmad S (2021) Injectable, self-healing, and biocompatible N, O-carboxymethyl chitosan/multialdehyde guar gum hydrogels for sustained anticancer drug delivery. Biomacromol 22:23731
16. Ćorković I, Pichler A, Buljeta I, Šimunović J, Kopjar M (2021) Carboxymethylcellulose hydrogels: Effect of its different amount on preservation of tart cherry anthocyanins and polyphenols. Curr Plant Biol 28:100222
17. Guilherme MR, Aouada FA, Fajardo AR, Martins AF, Paulino AT, Davi MFT, Rubira AF, Muniz EC (2015) Superabsorbent hydrogels based on polysaccharides for application in agriculture as soil conditioner and nutrient carrier: A review. Eur Polym J 72:365
18 Singh B, Sharma V, Rohit, Kumar A (2021) Designing moringa gum-sterculia gum-polyacrylamide hydrogel wound dressings for drug delivery applications. Carbohydr Polym Techn Appl 2:100062
19. Li F, Jin Y, He S, Jin J, Wang Z, Khan S, Tian G, Liang X (2021) Use of polyacrylamide modified biochar coupled with organic and chemical fertilizers for reducing phosphorus loss under different cropping systems. Agr Ecosyst Environ 310:107306
20. Alharbi K, Ghoneim A, Ebid A, El-Hamshary H, El-Newehy MH (2018) Controlled release of phosphorous fertilizer bound to carboxymethyl starch-g-polyacrylamide and maintaining a hydration level for the plant. Int J Biol Macromol 116:224
21. Hao Q, Chen T, Wang R, Feng J, Chen D, Yao W (2018) A separation-free polyacrylamide/bentonite/graphitic carbon nitride hydrogel with excellent performance in water treatment. J Clean Prod 197:1222
22. Alam A, Kuan HC, Zhao Z, Xu J, Ma J (2017) Novel polyacrylamide hydrogels by highly conductive, water-processable graphene. Compos Part A Appl S 1:93

23. Junior CRF, Tanaka FN, Bortolin A, Moura MR, Aouada FA (2018) Thermal and morphological characterization of highly porous nanocomposites for possible application in potassium controlled release. J Therm Anal Calorim 131:2205
24. Nascimento DWS, Moura MR, Mattoso LHC, Aouada FA (2017) Hybrid biodegradable hydrogels obtained from nanoclay and carboxymethylcellulose polysaccharide: Hydrophilic, kinetic, spectroscopic and morphological properties. J Nanosci Nanotechno 17:821
25. Shang XY, Zhao K, Qian WX, Zhu QY, Zhou GQ (2020) On the calculation of van der Waals force between clay particles. Minerals 10:993
26. Soleimani M, Siahpoosh ZH (2016) Determination of Cu(II) in water and food samples by Cloisite-Na^+ nanoclay as a new adsorbent: Equilibrium, kinetic and thermodynamic studies. J Taiwan Inst Chem E 59:413
27. Mallakpour S, Behnamfar MT, Dinari M, Hadadzadeh H (2015) Preparation of new fluorophore lanthanide complexes-Cloisite nanohybrids using the tricationic Pr(III), Gd(III) and Dy(III) complexes with 9,10-phenanthrenequinone. Spectrochimica Acta A 137:1206
28. Zhang S, Shi Z, Xu H, Ma X, Yin J, Tian M (2016) Revisiting the mechanism of redox-polymerization to build the hydrogel with excellent properties using a novel initiator. Soft Matter 12:2575
29. Bel'nikevich NG, Boborva NV, Elokhovckii VY, Zoolshoev ZF, Smirnov MA, Elyashevich GK (2011) Effect of initiator on the structure of hydrogels of cross-linked polyacrylic acid. Russ J Appl Chem 84:2106
30. Orakdogen N, Okay O (2007) Influence of the initiator system on the spatial inhomogeneity in acrylamide-based hydrogels. J Appl Polym Sci 103:3228
31. Wilems TS, Lu X, Kurosu YE, Khan Z, Lim HJ, Callahan LAS (2017) Effects of free radical initiators on polyethylene glycol dimethacrylate hydrogel properties and biocompatibility. J Biomed Mater Res Part A 105:3059
32. Agarwal P, Greene DG, Sherman S, Wendl K, Vega L, Park H, Shimanovich R, Reid DL (2021) Structural characterization and developability assessment of sustained release hydrogels for rapid implementation during preclinical studies. Eur J Pharm Sci 158:105689
33. Junior CRF, Fernandes RS, Moura MR, Aouada FA (2020) On the preparation and physicochemical properties of pH-responsive hydrogel nanocomposite based on poly(acid methacrylic)/laponite RDS. Mater Today Commun 23:100936
34. Shah R, Saha N, Saha P (2015) Influence of temperature, pH and simulated biological solutions on swelling and structural properties of biomineralized ($CaCO_3$) PVP–CMC hydrogel. Prog Biomater 4:123
35. Ritger PL, Peppas NA (1987) Simple equation for description of solute release I. Fickian and non-Fickian release from non-swellable devices in the form of slabs, spheres, cylinders or discs. J Control Release 5:23
36. Fernandes RS, Tanaka FN, Moura MR, Aouada FA (2019) Development of alginate/starch-based hydrogels crosslinked with different ions: hydrophilic, kinetic and spectroscopic properties. Mater Today Commun 21:100636
37. Varaprasad K, Jayaramudu T, Sadiku ER (2017) Removal of dye by carboxymethyl cellulose, acrylamide and graphene oxide via a free radical polymerization process. Carbohydr Polym 164:186
38. Aouada FA, Bortolin A, Moura MR, Longo E, Mattoso LHC (2012) Synthesis and characterization of novel pH sensitive PAAm-PMAA-CMC hydrogels and their applications in the controlled release of fertilizer. In: Hydrogels: Synthesis, characterization and applications. Nova Science Publishers, New York, pp 279–298
39. Tanaka FN, Junior CRF, Moura MR, Aouada FA (2018) Water absorption and physicochemical characterization of novel zeolite-PMAA-co-PAAm nanocomposites. J Nanosci Nanotechno 18:7286
40. Xiong J, Li Q, Shi Z, Ye J (2017) Interactions between wheat starch and cellulose derivatives in short-term retrogradation: Rheology and FTIR study. Food Res Int 100:858
41. Ma J, Xu Y, Fan B, Liang B (2007) Preparation and characterization of sodium carboxymethylcellulose/poly(N-isopropylacrylamide)/clay semi-IPN nanocomposite hydrogels. Eur Polym J 43:2221
42. Fernandes RS, Moura MR, Glenn GM, Aouada FA (2018) Thermal, microstructural, and spectroscopic analysis of Ca^{2+} alginate/clay nanocomposite hydrogel beads. J Mol Liq 265:327
43. Junior CRF, Moura MR, Aouada FA (2017) Synthesis and characterization of intercalated nanocomposites based on poly(methacrylic acid) hydrogel and nanoclay cloisite-na^+ for possible application in agriculture. J Nanosci Nanotechno 17:5878
44. Mirzataheri M, Khamisabadi S, Salimi A (2016) Characterization of styrene-co-butyl acrylate/Cloisite-Na^+ nanocomposite film synthesized via soap free emulsion polymerization. Prog Org Coat 99:274
45. Brantseva T, Antonov S, Kostyuk A, Ignatenko V, Smirnova N, Korolev Y, Tereshin A, Ilyin S (2016) Rheological and adhesive properties of PIB-based pressure-sensitive adhesives with montmorillonite-type nanofiller. Eur Polym J 76:228
46. Aouada FA, Pan Z, Orts WJ, Mattoso LHC (2009) Removal of paraquat pesticide from aqueous solutions using a novel adsorbent material based on polyacrylamide and methylcellulose hydrogels. J Appl Polym Sci 114:2139
47. Saputra AH, Hapsari M, Pitaloka AB, Wulan PPD (2015) Synthesis and characterization of hydrogel from cellulose derivatives of water hyacinth (*Eichhornia crassipes*) through chemical cross-linking method by using citric acid. J Eng Sci Technol 21:75
48. Meng Z, Wang M, Cao X, Wang T, Wang Y, Xu Y, Liu W, Chen L, Huang Y, Liu X (2022) Highly flexible interconnected Li+ ion-sieve porous hydrogels with self-regulating nanonetwork structure for marine lithium recovery. Chem Eng J 445:136780
49. Cao H, Ma X, Wei Z, Tan Y, Chen S, Ye T, Yuan M, Yu J, Wu X, Yin F, Xu F (2022) Behavior and mechanism of the adsorption of lead by an eco-friendly porous double-network hydrogel derived from keratin. Chemosphere 289:133086
50. Tang H, Chen H, Duan B, Lu A, Zhang L (2014) Swelling behaviors of superabsorbent chitin/carboxymethylcellulose hydrogel. J Mater Sci 49:2235
51. Umar A, Naim AA, Sanagi MM (2014) Synthesis and characterization of chitosan grafted with polystyrene using ammonium persulfate initiator. Mater Lett 124:12
52. Naim AA, Umara A, Sanagib MM, Basaruddina N (2013) Chemical modification of chitin by grafting with polystyrene using ammonium persulfate initiator. Carbohydr Polym 98:1618
53. Coutinho FMB, Oliveira CMF (2006) Reações de polimerização em cadeia – Mecanismo e Cinética, 1edn. Interciência, Rio de Janeiro
54. Xiang H, Xia M, Cunningham A, Chen W, Sun B, Zhu M (2017) Mechanical properties of biocompatible clay/P(MEO_2MA-co-OEGMA) nanocomposite hydrogels. J Mech Behav Biomed Mater 72:74
55. Aouada FA, Chiou BS, Orts WJ, Mattoso LHC (2009) Physicochemical and morphological properties of poly(acrylamide) and methylcellulose hydrogels: Effects of monomer, crosslinker and polysaccharide compositions. Polym Eng Sci 49:2467
56. Parlato M, Murphy W (2014) Soluble molecule transport within synthetic hydrogels in comparison to the native extracellular matrix. In: Hydrogels in cell-based therapies. RSC Soft Matter, pp 1–30
57. Li Y, Xiunan L, Chen C, Zhao D, Su Z, Ma G (2016) A rapid, non-invasive and non-destructive method for studying swelling behavior and microstructure variations of hydrogels. Carbohydr Polym 151:1251